Vaporization of Prostatic Tissue to Treat Benign Prostatic Hyperplasia

BEE 4530: Computer Aided Engineering

Group 3:
Dan Currie
Elaina Griffo
Jin Kim
Sarah Wheeling

Table of Contents

1. Executive Summary

The prostate is a key component of the male reproductive system. Often, due to age, the prostate becomes enlarged resulting in a condition known as Benign Prostatic Hyperplasia (BPH). While pharmacological options are generally the first choice, surgery is sometimes necessary to treat this condition. Laser procedures are ideal because of the decreased risks to the patient, but complications arise when the layer of coagulated tissue created by the laser becomes too thick. An ideal laser wattage and application time must be determined in order to minimize the coagulation layer while achieving an effective level of vaporization. The goal of this simulation was to create a model from which an ideal set of laser parameters for the laser treatment of BPH can be determined. This was achieved using finite-element analysis of the laser heating of a 2-dimensional axisymmetric prostate model using COMSOL Multiphysics software. Using this simulation, the vaporization and coagulation thicknesses in prostatic tissue treated for 5 seconds with a 40W, 80W, or 120W laser, or treated for 1 second with a 60W, 80W or 120W laser were determined. The results indicated that increasing laser wattage and/or application time increases the thickness of vaporized tissue and decreases the thickness of coagulation. Furthermore, the results suggested that the thickness of the coagulation zone converges to a minimum value as wattage and/or application time is increased. This simulation was preliminary; however, this model can ideally be used to determine an ideal laser wattage-application time combination that produces the desired level of vaporization while minimizing tissue coagulation.

2. Introduction

2.1 Background Information

Located below the bladder surrounding the urethra, the prostate gland is an essential component of the male reproductive system. A normal prostate is slightly larger than a walnut; measuring, on average, 4.4 cm across, 2.6 cm from front to back, and 3.4 cm in length and weighing about 20 grams (+/- 6 grams) between ages 21 and 30[1,2]. In the absence of complications, the prostate will remain this size for the duration of a lifespan [2].

Unfortunately, a significant portion of the male population above the age of 50 will experience some kind of prostatic complications. Age related prostatic enlargement, often referred to as Benign Prostatic Hyperplasia (BPH), can begin after age thirty and is estimated to effect between 8-20% of the male population in their forties, and 50% of the male population over 50 [2,3]. The histology of BPH is characterized by the growth of nodules within the prostate, which can lead to compression of the urethra due to barriers to outward growth [1,3]. In some cases this compression is mild with no bothersome symptoms, but in obstructive cases BPH can interfere with normal urination or in extreme cases completely block the urethral canal. BPH becomes a clinical problem when patients develop bothersome symptoms, which include difficulty in or inability to completely empty the bladder, hesitancy (difficulty beginning to urinate), weak stream, incontinence, and urinary tract infections [3]. The American Urological Association has established a reliable symptom index for BPH which includes seven questions relating to frequency, nocturia, weak urinary stream, hesitancy, intermittence, incomplete emptying and urgency [4]. These clinical symptoms are collectively referred to as lower urinary tract symptoms (LUTS) and manifest in approximately 50% of men with histological evidence of BPH [3].

The range of severity in BPH symptoms and their impact on daily life leads to a similar diversity in treatment strategies. For example, in mild cases, BPH is often treated with 'watchful waiting' and frequent reassessment of symptoms, whereas the most obstructive cases require some type of surgical intervention [3]. Pharmacological strategies, such as administration of alpha blockers or 5-alpha reductase inhibitors, are also commonly used to manage BPH [3]. The disadvantage to alpha blockers, which work by relaxing smooth muscle to relieve LUTS, is their potential to cause hypotension as they do not discriminately affect the smooth muscle of the bladder and urethra and can also affect vascular smooth muscle[3]. When medical interventions prove unsuccessful surgical procedures are considered. Transurethral resection of the prostate (TURP) is the surgical removal of prostate tissue using electrocautery or dissection. TURP is the standard surgical treatment of BPH due to the substantial data confirming its efficacy [3]. However, TURP has significant disadvantages. As with any surgical procedure, TURP requires anesthesia and may cause bleeding as well as an electrolyte imbalance due to the use of a bladder irrigant[3]. Long-term complications include sexual dysfunction and the need for reoperation within two years for 2 out of 30 TURP patients [3]. Due to these disadvantages, effective alternatives to TURP are in demand and many are being used today.

Laser procedures are a desirable surgical alternative to TURP as they achieve similar results with a lower tendency for bleeding and less post procedure morbidity[3]. Various effective laser procedures exist, but complications still arise when the laser procedure produces a thick coagulation zone. For example, an Nd:YAG laser vaporizes only a small amount of tissue and induces deep coagulation which can cause accumulation of fluid and prolonged urinary retention[5]. Therefore, of particular interest is laser prostatectomy using a green light laser, also known as photoselective vaporization of the prostate (PVP)[6]. The aim of PVP is to selectively vaporize a region of the enlarged prostate tissue to alleviate obstruction of the urethra. PVP results in a thin (1-2 mm) coagulation zone which is successful in sealing blood vessels and

preventing the problems associated with an Nd:YAG laser[5]. PVP has been demonstrated to be as or more effective than alternative procedures, with persistent results (up to 5 years post procedure) and less complications[6]. This long-term efficacy may be the final evidence needed for PVP to replace TURP as the standard surgical treatment for BPH. As a result, it is critical to examine the PVP procedure and understand the implications it may have on the future of BPH treatment.

2.2 Design Objectives

Vaporization of tissue occurs due to boiling of water within the tissue and the resulting pressure of water vapor bubbles on the collagen matrix. Therefore, for tissue to be vaporized the temperature must reach 100^{o}C. Coagulation of tissue occurs when proteins in the tissue denature, which occurs between 60-65^{o}C. Coagulation is important as it helps seal the tissue to prevent bleeding, but when coagulated tissue becomes too thick it can lead to complications. The PVP laser procedure produces only a thin layer of coagulation beyond the vaporized region. This is particularly effective, as it limits some of the post surgery problems associated with necrotic tissue produced in laser procedures that aim to cause only coagulation of the tissue.

Our main objective is to model the effects of a PVP procedure using a high power potassium-titanyl phosphate (KTP) green light laser on the tissue of an enlarged prostate. Specifically, our goal is to examine the effects of various laser wattages and application times on the temperature, vaporization depth, and coagulation zone thickness of the prostate and surrounding tissue. We aim to determine the quantitative effects of: (1) increasing laser wattage from 40 to 120W, and (2) increasing application time from 1 to 5 seconds

2.3 Problem Schematic

For the purposes of modeling the KTP laser surgery the walnut shaped prostate was approximated as a cylinder. This approximation created axisymmetry about the z axis and lateral symmetry about the r axis which enabled us to reduce the complexity of our model by focusing on one quarter of the prostate (Figure 2.3.1(b))._

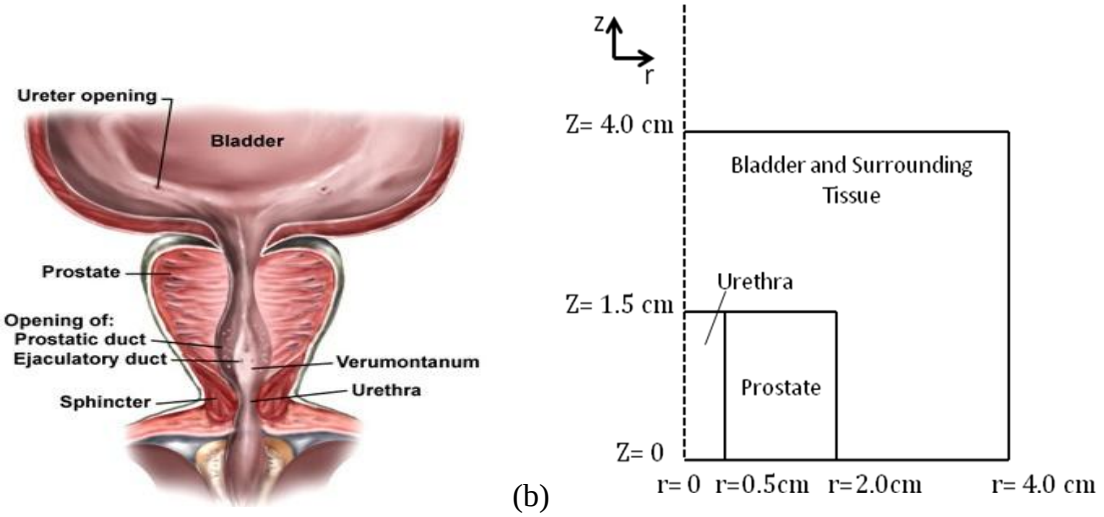

Figure 2.3.1. (a) Biological Schematic showing physical anatomy of the prostate. (b) Model schematic of the prostate and surrounding tissue with the prostate approximated as a cylinder with a diameter of 4 cm (including urethra) and height of 3 cm, and offset 2.5 mm from the z-axis to account for the urethra. There is 2D axisymmetry about the z-axis and lateral symmetry about the r-axis. (Note: schematic is not drawn to scale)

3. Results and Discussion

3.1 Mathematical Background

The governing equations used for our model included the transient heat transfer equation with a source term, the light diffusion equation, and a mass diffusion equation for moisture content (Appendix A). The heat transfer equation was used to solve for temperature within the computational domain. This required implementation of the light diffusion equation to find the fluence rate (φ) as the heat source term was defined as the product of the absorption coefficient (μ_a) and the fluence rate (φ). Finally, a mass diffusion model was used to determine the moisture content of the tissue as it affects the absorption coefficient (μ_a), and therefore, the heat source term. Further information on the solution strategy, such as the software used or meshing, can be found in Appendix B.

3.2 Temperature Profile

The completion of this model gives a quantitative look at KTP laser surgery. For a preliminary test, an 80 W laser power with a 1 second run time was used to obtain a spatial image of the temperature of the prostate. Only a small region of the prostate and surrounding was heated above the vaporization temperature of 373 K (Figure 3.2.1). Under these conditions, approximately 1.17 mm of the prostate tissue was vaporized and damage to the surrounding tissue was limited to a small region where the prostate and surrounding tissue meet (Figure 3.2.2.).

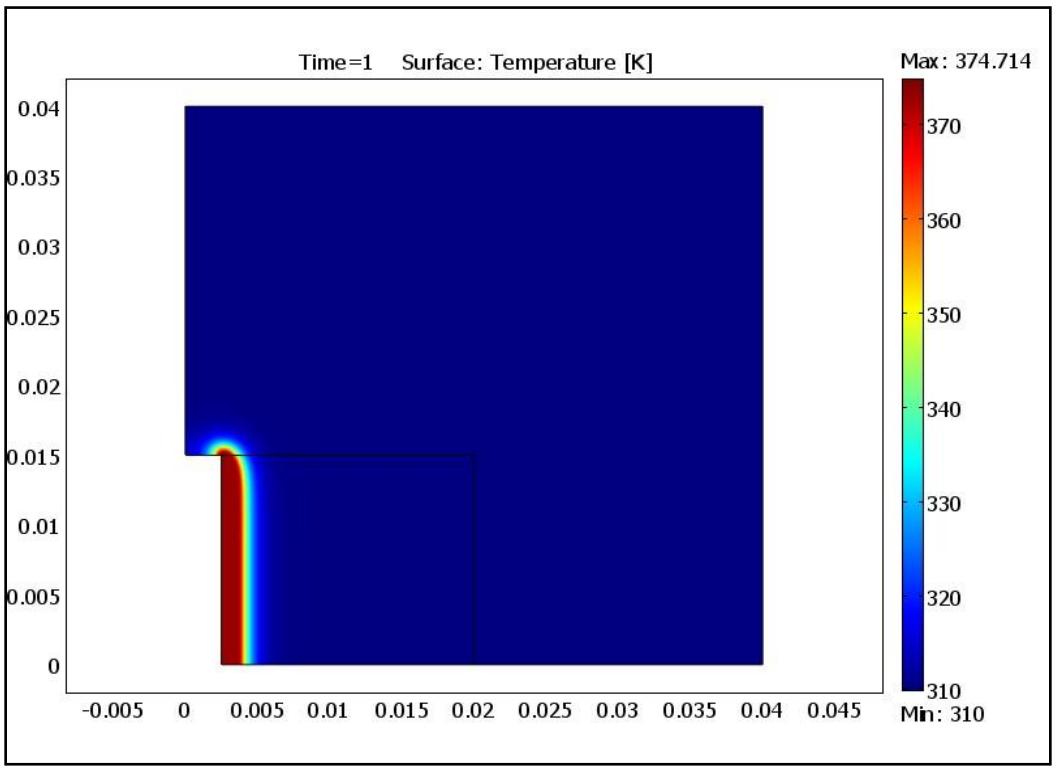

Figure 3.2.1. Surface Plot of Model: Plot of temperature after 1 second of heating at 80W. This plot shows that a small section of the prostate region adjacent to the urethra is heated with minimal heating in the surrounding tissue. A small portion of the surrounding tissue above the prostate urethra interface is heated.

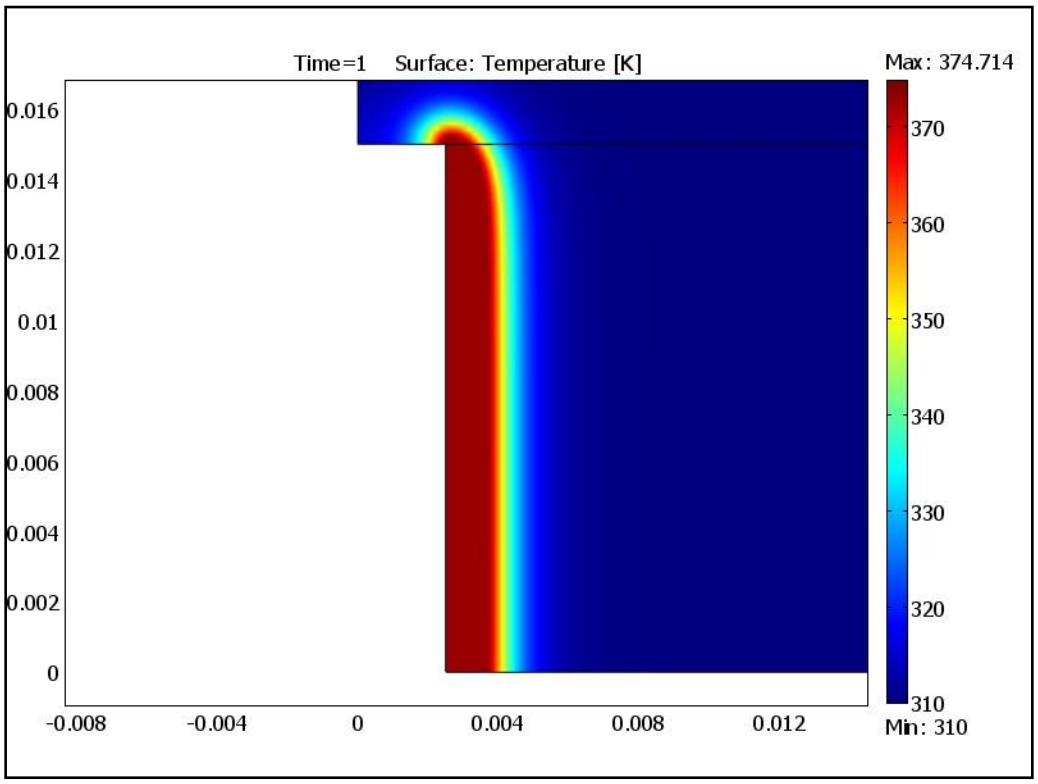

Figure 3.2.2. Surface Plot of Prostate: Close up of the heated prostate region after 1 second of heating at 80W. This shows an ablation region of the prostate adjacent to the urethra that is heated to approximately 373K. Past this region there is a temperature gradient and then the surrounding tissue and majority of the prostate is still at the initial temperature of 310K.

The maximum temperature in the prostate is approximately 373K. This temperature is just high enough to vaporize the tissue (Figure 3.2.2). For the 80W laser the surrounding tissue directly above the prostate is being heated to a maximum temperature of 374.7K. This is misleading because the moisture content equation is not being implemented in the surrounding tissue due to the extremely long running time. If the vaporization of the water in the surrounding tissue were being accounted for, the maximum temperature would be significantly lower and there would be minimal damage to this tissue. Additionally, a point in the prostate tissue was selected and a plot of the change in temperature over the run time was created (Figure 6.3.1). The temperature change with time is fairly linear, with an approximate increase of 10 degrees/second.

Furthermore, to examine the role that moisture content played in the temperature profile the moisture content of the prostate after 1 second of laser heating at 80 W was plotted (Figure 6.3.2). As expected, the moisture content dropped dramatically in the ablated region of the prostate and remained constant in the majority of the prostate tissue.

3.3 Vaporization and Coagulation Zones

To elucidate the vaporization zone versus the coagulation zone, a contour plot was created (Figure 3.3.1). The first contour line is at 373 K, showing the section of prostate vaporized. The other two contour lines are at 338 and 333 K showing the range of thicknesses of prostate coagulation. Because tissue coagulation causes severe negative side effects, coagulation thickness was calculated using the 333K contour to determine the maximum possible coagulation thickness. Therefore, coagulation thickness was defined as the distance between the 333 K contour and the 373 K contour corresponding to the edge of the vaporization zone.

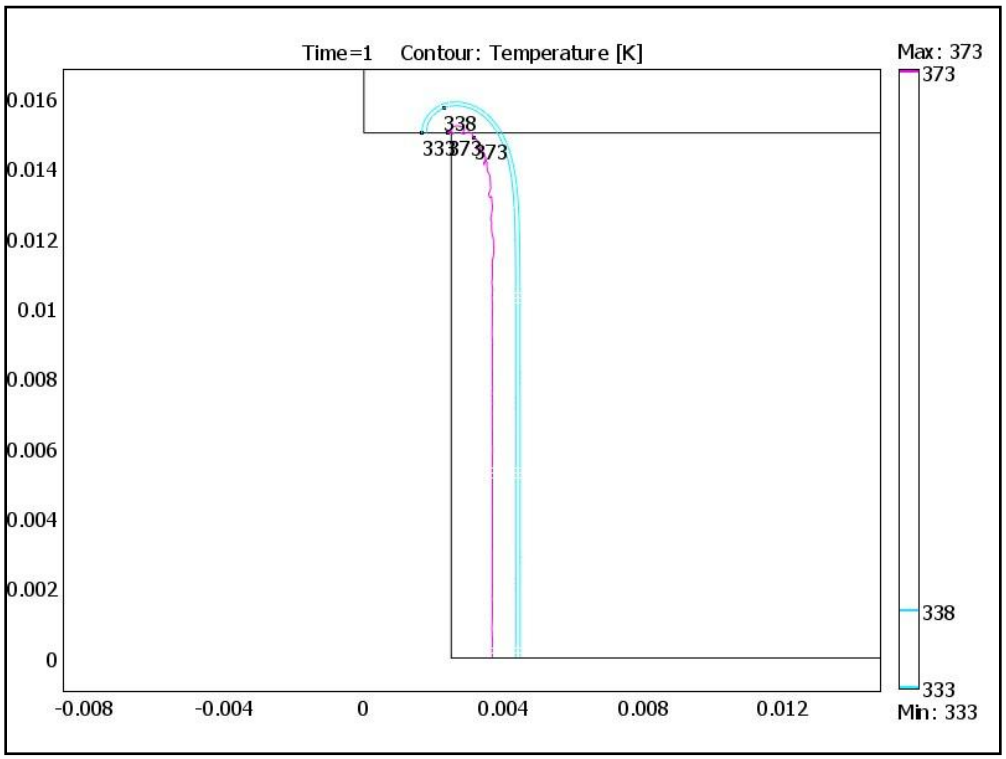

Figure 3.3.1. Coagulation and Vaporization Zones: Contour plot of prostate region at 1 second at 80W, showing contours at 333 K, 338 K, and 373 K, which correspond to coagulation and vaporization temperatures. Vaporization depth was determined to be 1.17 mm and the coagulation depth was 0.795 mm.

3.4 Wattage and Run Time Variation

To further understand the effects of laser wattage and application time on KTP laser surgery the model was run with variations in these two parameters. First, laser wattage was changed to 60W or 120 W with a 1 second run time. The contour plots for these wattages can be found in Appendix C (Figures 6.3.3 and6.3.4). Next, the run time was increased to 5 seconds with laser wattages of 40, 80, and 120 W. In this case, 40W was used instead of 60W to facilitate validation of the model, which is discussed further in section 3.5. The contour plots for these runs can be found in Appendix C (Figure 6.3.5 through 6.3.7). As expected, vaporization thickness, defined as the distance between the prostate edge and the 373 K contour, increased as laser wattage increased (Figure 3.4.1). Additionally, vaporization thickness increased as application time increased (Figure 3.4.1). However, coagulation thickness, defined as the distance between the 333 K contour and the 373 K contour, decreased as laser wattage increased (Figure 3.4.2). For identical wattages coagulation thickness increased as application time increased, but at higher wattages, the difference between the 1 second and 5 second coagulation thicknesses decreased (Figure 3.4.2). This indicates that coagulation zone thickness converges to a minimum and is unavoidable, which is ideal as coagulation is necessary to seal the tissue at the edge of the vaporization zone and prevent bleeding.

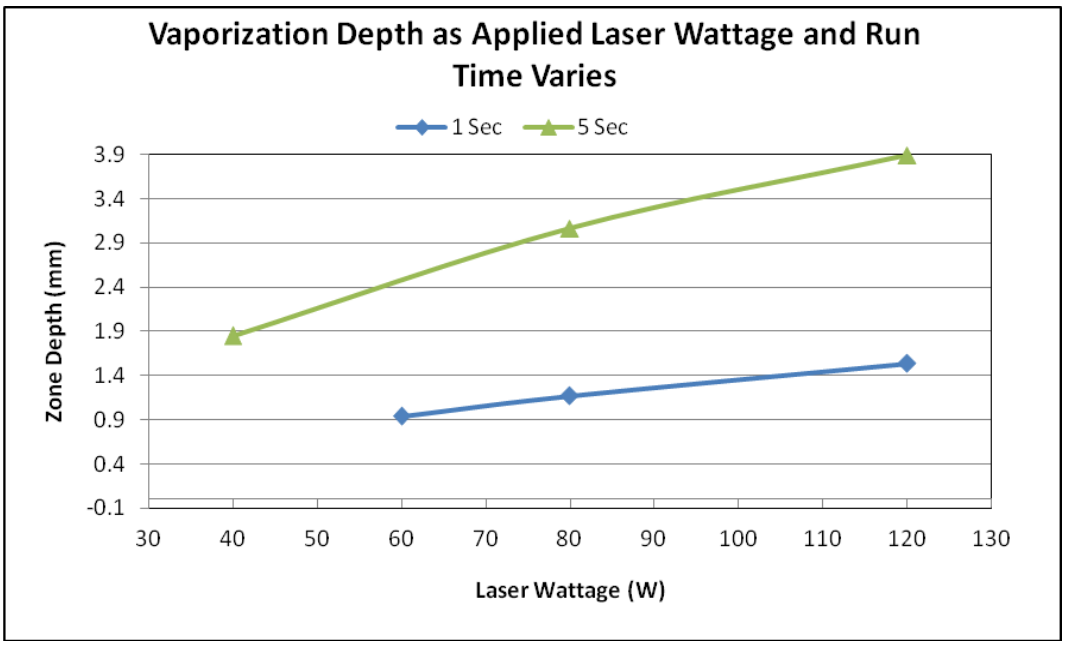

Figure 3.4.1. Vaporization Depth: Trends in the depth of the vaporization zone of the prostate as the laser wattage and run time parameters are varied.

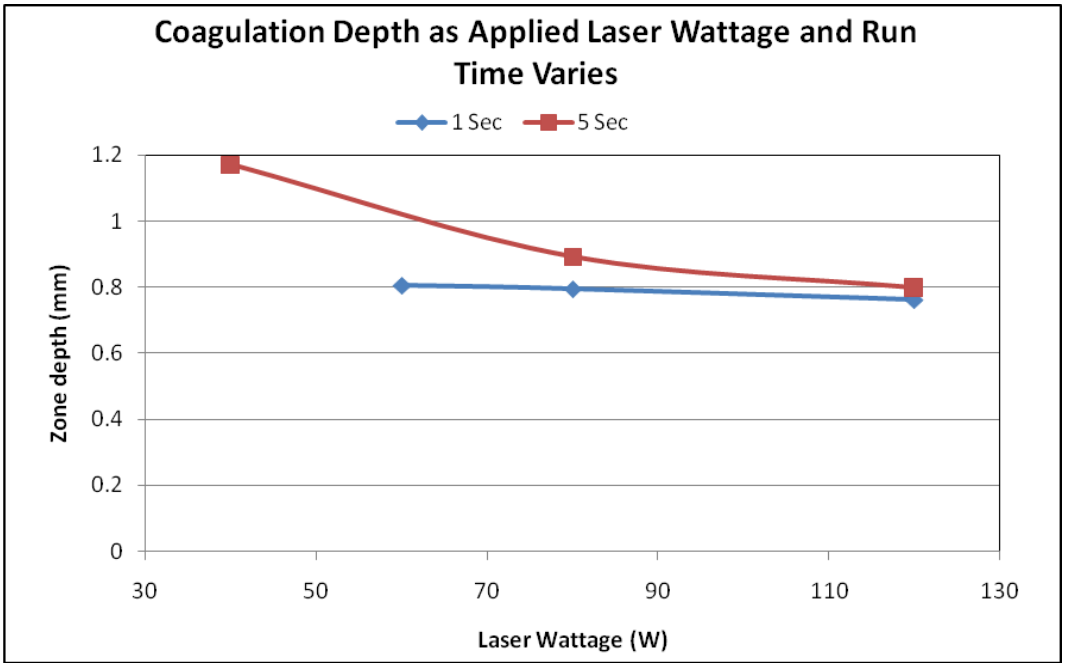

Figure 3.4.2. Coagulation Depth: Trends in the depth of the coagulation zone of the prostate as the laser wattage and run time parameters are varied.

3.5 Validation

To validate the model, its results were compared to experimental results of previous research on the effects of laser heating of canine prostate tissue.[17] The experimental results were obtained by measuring the vaporization and coagulation thicknesses in canine prostate tissue treated with 40, 80, and 120W lasers for 5 seconds[17]. These values were plotted against the coagulation and vaporization thicknesses determined by simulation of similar procedures using the model(Figures 3.5.1 and 3.5.2).

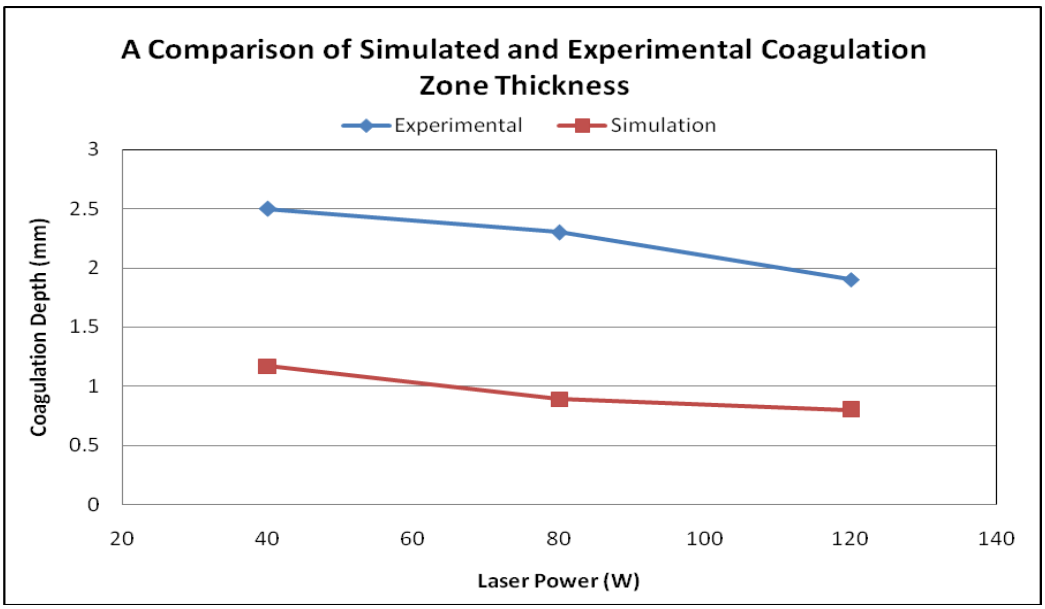

Figure 3.5.1. Coagulation Thickness Validation: The simulated and experimental coagulation thicknesses in the prostate after 5 seconds with laser powers of 40, 80, and 120W.

In both the experimental and the simulated data, there is a decreasing trend in the coagulation thickness as the laser power increases. The simulated coagulation thicknesses, however, are all at least 1 mm smaller than the experimental values (Figure 3.5.1).

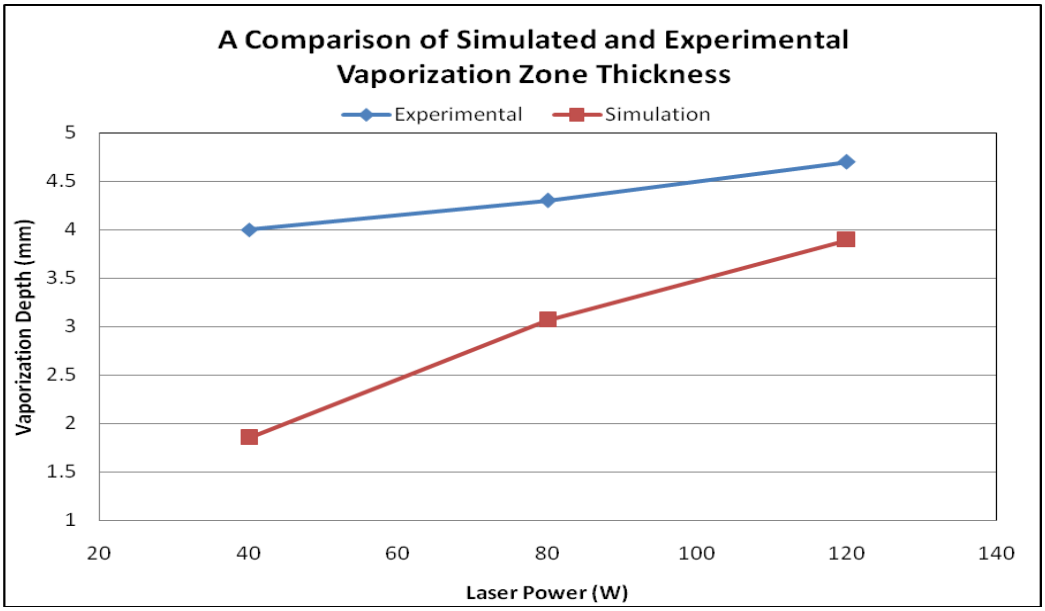

Figure 3.5.2. Vaporization Thickness Validation: The simulated and experimental vaporization thicknesses in the prostate after 5 seconds with laser powers of 40, 80, and 120W.

In both the simulation and the experimental data the vaporization thickness increases with laser power. The simulated thickness is more than 2mm less than the experimental thickness at a laser power of 40W, but this difference decreases to slightly larger than 1mm as the power is increased to 120W (Figure 3.5.2). Some of the differences between the simulated and experimental values may be caused by the differences between human and canine prostate tissue properties, since human tissue properties were used in the simulation but the experiment was performed on canine tissue.

3.6 Sensitivity Analysis

Since accurate property data are not always available, a sensitivity analysis was performed to examine the effects of parameter variability. Tissue parameters, such as density, specific heat capacity, and thermal conductivity were varied by +/- 10% from their original value. This indicated which parameters were sensitive to changes and how variation in parameter values affected the objective function: average prostate tissue temperature (Figure 3.6.1).

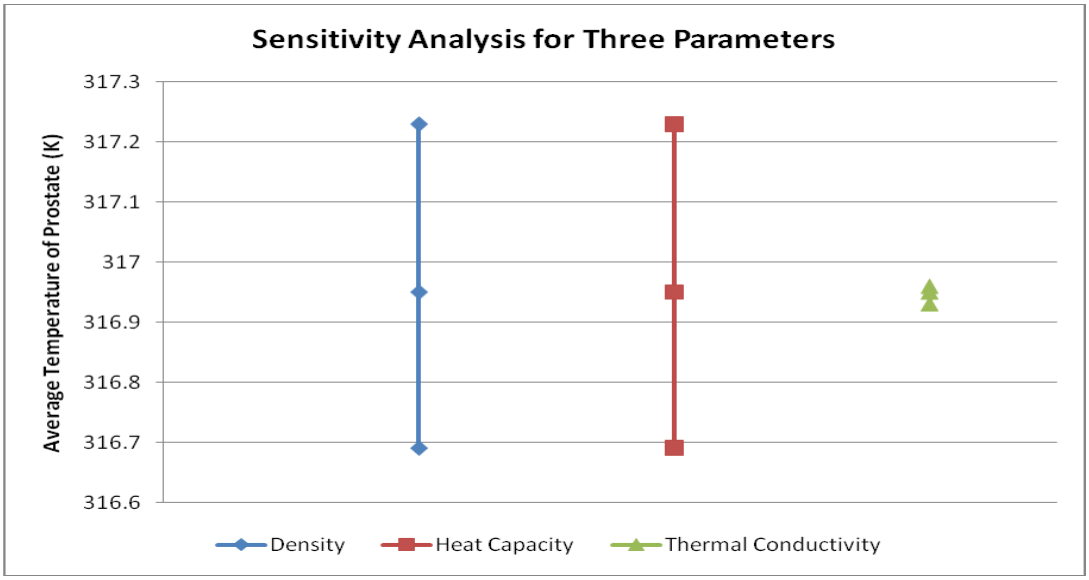

Figure 3.6.1. Sensitivity Analysis: Analysis for density, heat capacity, and thermal conductivity, varying each parameter by +/- 5% and +/- 10% to obtain the effect this had on average prostate temperature.

Changes in both the density and the heat capacity had a noticeable and equivalent effect on the average prostate temperature (Figure 3.6.1). This is intuitive, since these parameters are multiplied together in the governing equation. The total variation between -10% and +10% for both the density and the heat capacity is .54K, with the average temperature decreasing with increasing parameter values (Figure 3.6.1). The thermal conductivity affected the average prostate temperature minimally, with a difference of only .03K between the -10% and +10% values (Figure 3.6.1). This analysis indicated that larger importance needed to be placed on accurate density and heat capacity values as their variation resulted in larger temperature variation.

4. Conclusions and Design Recommendations

4.1 Conclusions

The primary objective of this project was to model the effects of a PVP procedure on an enlarged prostate using a KTP laser. Using COMSOL, the effect of an 80W KTP laser targeting an enlarged prostate was modeled to find its effect on the temperature, thickness of coagulation, and thickness of vaporization in the prostate. Simulation of an80 W laser applied for 1 second indicated that a small portion of the prostate reached a maximum temperature of 373 K, while the rest of the prostate along with the surrounding tissue remained at the initial temperature of 310 K (Figure 3.2.2). The contour plot showed a coagulation thickness of 0.795 mm and a vaporization thickness of 1.17 mm (Figure 3.3.1). Additionally, by running the model for different laser powers, i.e. 40 W, 60 W, and 120 W, with run times of 1 second and 5 seconds, it was concluded that both coagulation and vaporization thicknesses were dependent on the magnitude of laser wattage. More specifically, coagulation depth decreased with increased laser wattage and vaporization depth increased with increased laser wattage. Comparing the coagulation thicknesses with respect to run time, the coagulation depths for a run time of 5 seconds were slightly larger (by less than a factor of 1), yet nearly equivalent to the coagulation depths for a run time of 1 second. On the other hand, the vaporization depths for a run time of 5 seconds were about twice to three times greater in magnitude than those for a run time of 1 second. Such behavior could be due to the fact that as run time was increased, the laser emitted thermal energy for a longer period of time on the prostate, and therefore, heat input to the prostate increased, which led to greater degrees of vaporization.

Results from conducting a sensitivity analysis for the three parameters, density, heat capacity, and thermal conductivity, indicated that changes in thermal conductivity had minimal effects on the average temperature of a prostate, while changes in density and heat capacity values had significant effects, both of which had average prostate temperatures that were extended over a range of 316.69 K to 317.23 K. In order to check the accuracy and validity of our model, we referenced past research conducted on laser treatment of the prostate in a canine model by Lee, et. al (2008). Although this particular source does not focus on a human prostate, model parameters, such as the type of laser used, laser wattages, and run time, were comparable to the parameters that were used in this model. Because of such similarities, this research paper was used as a validation source for which the model's results could be compared and accuracy could be checked. Validations revealed that both the simulated and experimental results for coagulation and vaporization thicknesses followed the same trend, but differed in thickness magnitude by factors of two or smaller. The differences in magnitude occurred because of the slight differences in tissue properties between a human and canine prostate. The comparable data trends, however, verified the feasibility and correctness of the model.

4.2 Design Recommendations

(1) Model the prostate with the "walnut" geometry. The prostate model that we have created using the COMSOL software is a simplified two-dimensional model representing the structural and functional physics of a genuine prostate approximated as a cylinder to simplify the geometry. To have a more accurate model, it would be necessary to take into account the "walnut" geometry of the prostate and to model it accordingly with attention to such fine details.

(2) Include fluid flow mechanism that mimics and is comparable to a continuous bladder irrigation system that provides a cooling effect to the prostate's surrounding tissue so that the thermal energy given off by the KTP laser does not raise the temperature of or harm the surrounding healthy tissue regions.

5. Discussion of Project Constraints

5.1 Economic Constraints

KTP laser treatment for benign prostatic hyperplasia is a fairly expensive medical treatment. The cost for this medical treatment, however, is still lower than the costs for comparable treatments, such as transurethral prostatectomy[16]. BPH treatment using a KTP laser has been shown to have a success rate that is incomparable to any other BPH treatments. The minimal failure rates of this treatment make it economically efficient as re-treatments are not necessary. Taking into consideration the short and long-term costs, BPH treatment with the KTP laser is the least expensive and the most cost efficient.

5.2 Health and Safety Constraints

Similar to any other medical treatment or medical modeling, the safety of the patient is of utmost importance at all times, under any condition. One of the greatest advantages of this treatment method is the absence of blood during the surgical procedure since a laser is used to completely destroy the enlarged, excess prostate tissue. Although the patient does undergo operation, he or she will remain in a relatively healthy condition, considering the fact that blood loss does not occur. This non-invasive treatment greatly reduces post-operative health risks that could form with time after completion of the surgery. KTP laser prostatectomy is a method of high effectiveness, providing the patients with an excellent short and long-term functional outcome, whereas at the same time the method has a low morbidity [16].

A health problem that could arise from the medical procedure is the application of the laser. More specifically, laser wattage could be too strong or laser application time could be too long, or heat generated from the laser could be so high that this heat could diffuse to the surrounding region of healthy tissue. This could result in inadvertent coagulation and vaporization of healthy surrounding tissue, which is a specific problem that this model attempted to reduce and/or avoid.

5.3 Modeling Constraints

(1) Total amount of time for which the model can be run, as well as the size of the time steps. Because unlimited time is not provided, it is crucial to have the model successfully run within a desired range of time with time steps that are large enough so that the model can run at a quicker speed, but small enough so that the results are accurate.

(2) Difficulty in incorporating a continuous bladder irrigation system to the COMSOL model. In a real KTP laser treatment for BPH, the procedure not only focuses on laser application for tissue coagulation and ablation, but also uses a continuous bladder irrigation system. This irrigation system ensures that the high temperature heat directed to the prostate does not affect the surrounding tissue and provides a cooling effect for the tissue region surrounding the prostate. Such a bladder irrigation system is crucial for the cooling of surrounding tissues that could be heated due to the high temperature heat that is generated from the KTP laser targeting the prostate. Limited sources and knowledge of this system prohibited its inclusion in the model. With further background information of this system, the current model could be expanded to include irrigation and create a more complex, advanced, and accurate model in the future.

6. Appendices

6.1 Appendix A: Mathematical statement of the problem

Governing equations

Heat Transfer Equation (transient, conduction, source term):

$$\rho c_P \frac{\partial T}{\partial t} = k[\frac{1}{r}\frac{\partial}{\partial r}(r\frac{\partial T}{\partial r}) + \frac{\partial^2 T}{\partial z^2}] + Q \quad (1)$$

where:

$$Q = \mu_a \phi \quad (2)$$

To obtain the heat source term, Q, the heat source from light diffusion differential equation was solved for ϕ (3).

Heat Source from Light Diffusion:

$$\frac{\partial \phi}{\partial t} - D\nabla^2\phi + c_*\mu_a\phi = 0 \quad (3)$$

where :

$$D = c_*[3(\mu_a + (1-g)\mu_s)]^{-1} \quad (4)$$

Since vaporization of tissue is the result of vaporization of the water within the tissue, it causes a decrease in tissue moisture content. Also, the absorption (μ_a) and scattering (μ_s) coefficients, which govern the laser-tissue interaction, are determined primarily by the tissue's water content. To account for the effect of vaporization on the heat source term, the effect of moisture content on the absorption (μ_a) and scattering (μ_s) coefficients was considered. Since Q is directly proportional to μ_a and only indirectly related to μ_s through D, it was assumed that μ_a affects Q much more than μ_s. Thus, μ_s was assumed to remain constant and μ_a was assumed to vary linearly with moisture content such that μ_a equals zero when m equals zero and μ_a equals μ_{a0} when m equals m_0 (5).

$$\mu_a = \frac{m}{m_0}\mu_{a_0} \quad (5)$$

To obtain μ_a, an additional mass diffusion model was used to determine m, the moisture content of the tissue (6 & 7).

Mass Diffusion Model:

$$\delta_{ts} * \frac{\partial m}{\partial t} + \nabla \cdot (-D\nabla m) = R_{\mu_\alpha} \quad (6)$$

where:

$$R_{\mu_\alpha} = \left[\frac{-Q}{\lambda}\right] * (T > 373) \quad (7)$$

With δ_{ts} set to 1 and D equal to zero (no diffusion of moisture), this reduced to:

$$\frac{\partial m}{\partial t} = R_{\mu_a} \quad (8)$$

The reaction rate term, $R_{\mu a}$, relates the heat generated (Q) to the heat of vaporization (λ) giving the amount of water vaporized. Using the logic statement (T>373), a reaction rate was only present when the tissue temperature reached 100 C. In other words, initially heat was used to increase the temperature of the tissue to 100 C and any additional heat absorbed was used to evaporate the water in the tissue. These equations, therefore, model the effect that the moisture content has on Q, with μ_a modeled as a function of moisture content. As moisture content decreases μ_a also decreases. Due to the long solving times (90 minutes for our 1 second model), the moisture content diffusion model was not implemented in the surrounding tissue and μ_a was kept constant as μ_{a0}. The following three tables define the parameters (Table 6.1.1), the initial conditions (Table 6.1.2), and the boundary conditions (Table 6.1.3) that are used in the governing equations as described above.

Table 6.1.1. Input Parameters for COMSOL: Parameter symbols are defined in this table, as well as an indication of the source of the value or if it was solved for. The full references for these papers can be found in Appendix D.

	Parameter	**Value**	**Measurement Unit**	**Source**
ρ	Density	1090	kg/m^3	Zhang, et al
c_p	Heat Capacity	3500	J/kg ^oC	Zhang, et al
K	Thermal Conductivity	0.41	W/m ^oC	Zhang, et al
D	Optical Diffusion Coefficient	2.41E4	m^2/s	Solved
C_*	Speed of Light (in tissue)	2.18E8	m/s	Jacques
C_0	Speed of Light (in vacuum)	3.0E8	m/s	Zhang, et al
μ_a	Absorption Coefficient	236	m^{-1}	Zhang, et al
μ_s	Scattering Coefficient	13240	m^{-1}	Zhang, et al
G	Optical Anisotropy Factor	0.79	unitless	Zhang, et al
"	Spot Size	0.01	m	Zhang, et al
"	Spot Size Area	7.85398E-05	m^2	Zhang, et al
R	Reflection Ratio	0.1	unitless	Shafirstein
P(t)	Laser Irradiance	1018591.636	W/m^2	Elzayat
"	Applied Laser Power	80	W	Elzayat
"	Laser Wavelength	532	nm	Elzayat
Λ	Latent Heat of Water	40860	J/mol	Datta
m_0	Initial Moisture Content	42388.89	mol/m^3	Solved

Table 6.1.2. Initial Conditions.

Parameter	Prostate	Surrounding Tissue
T	310 K	310K
Φ	0	0
m	42388.89 mol/m^3	42388.89 mol/m^3

Table 6.1.3. Boundary Conditions.

Boundary	Heat Transfer (T)	Light Diffusion (φ)	Moisture (m)
Prostate/Urethra	Thermal Insulation	Equation (2)	Insulation
Vertical Axis	Axial Symmetry	Axial Symmetry	Axial Symmetry
All Other External	Thermal Insulation	Insulation	Insulation

6.2 Appendix B: Solution Strategy

The solution was implemented in COMSOL using three simultaneous governing equations, two for diffusion (water concentration and light concentration, phi) and one for heat transfer. A direct solver (UMFPACK) was used to solve these equations. Ten time steps of length 0.1s were taken between 0 and 1s. The relative and absolute tolerances were 0.01 and 0.001, respectively.

Initially a coarse mesh was used; however, the optimum mesh was determined by increasing the mesh until the solution converged (Figure 6.2.1). The final mesh consists of 6825 quadrilateral elements, with 425 boundary and 9 vertex elements (Figure 6.2.2).

The element quality of the final mesh is fairly high in the region of interest, the prostate, which suggests the values from these elements will be reasonable (Figure 6.2.3). The quality in parts of the surrounding tissue is low, but this is acceptable because the temperature in the tissue does not change significantly.

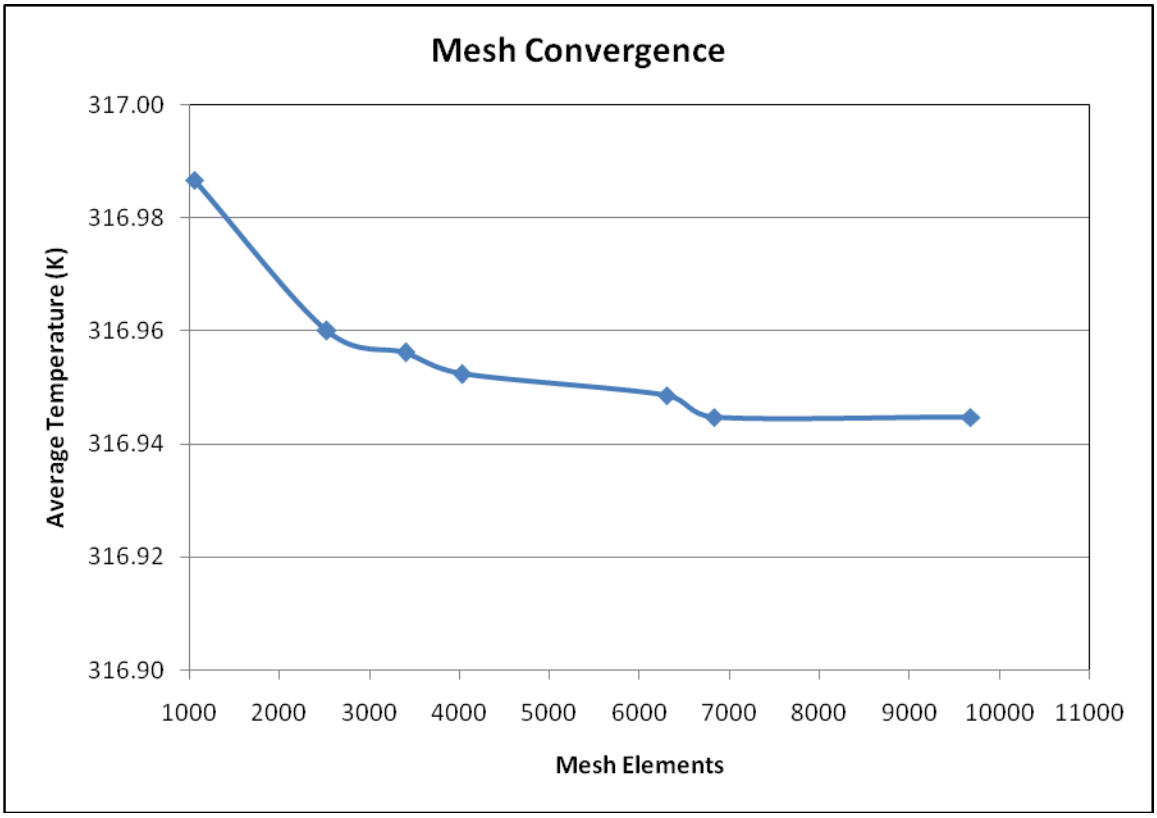

Figure 6.2.1. Mesh Convergence Analysis: By plotting the average temperature in the prostate with respect to the number of mesh elements, mesh convergence was obtained. The average temperature in the prostate remains constant between 6825 to 9675 mesh elements, which indicated that a converged solution has been achieved.

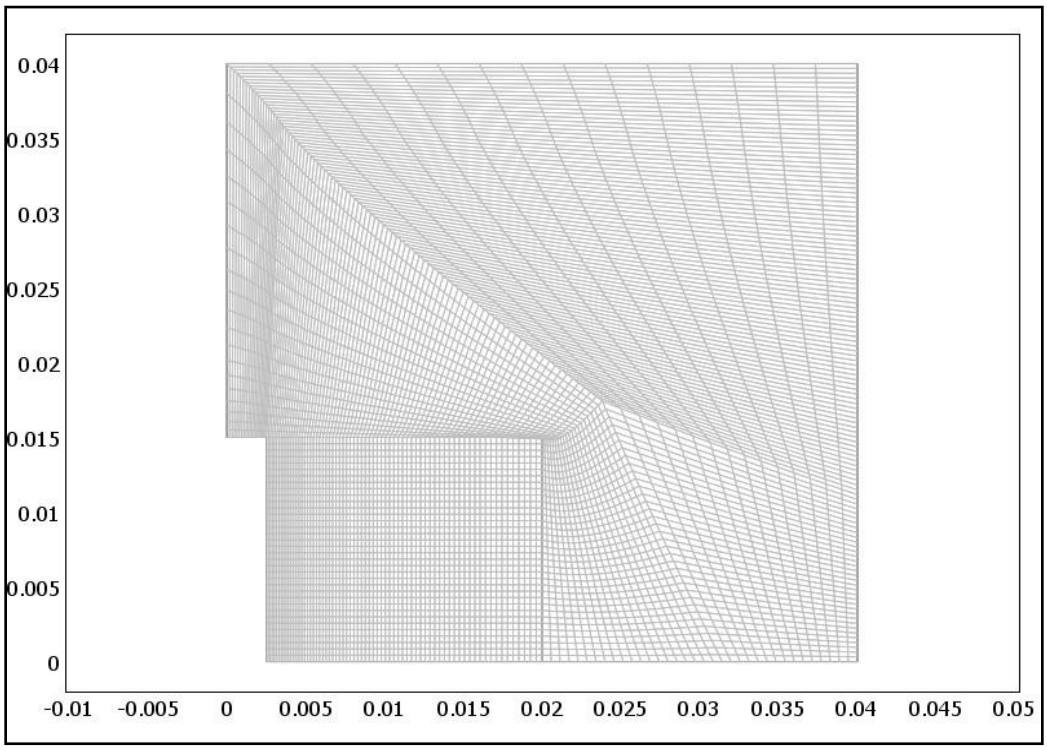

Figure 6.2.2. Domain Mesh: Simple mapped mesh created for subdomain 1 (surrounding) with a total of 4375 elements and an element area ratio of 0.0510 and subdomain 2 (prostate) with a total of 2450 elements and an element area ratio of 0.500. The left edge of the surrounding tissue and edge at the top of the urethra region have 20 elements, the left and right edges of the prostate have 35 elements, and the top and bottom edges of the prostate have 70 elements.

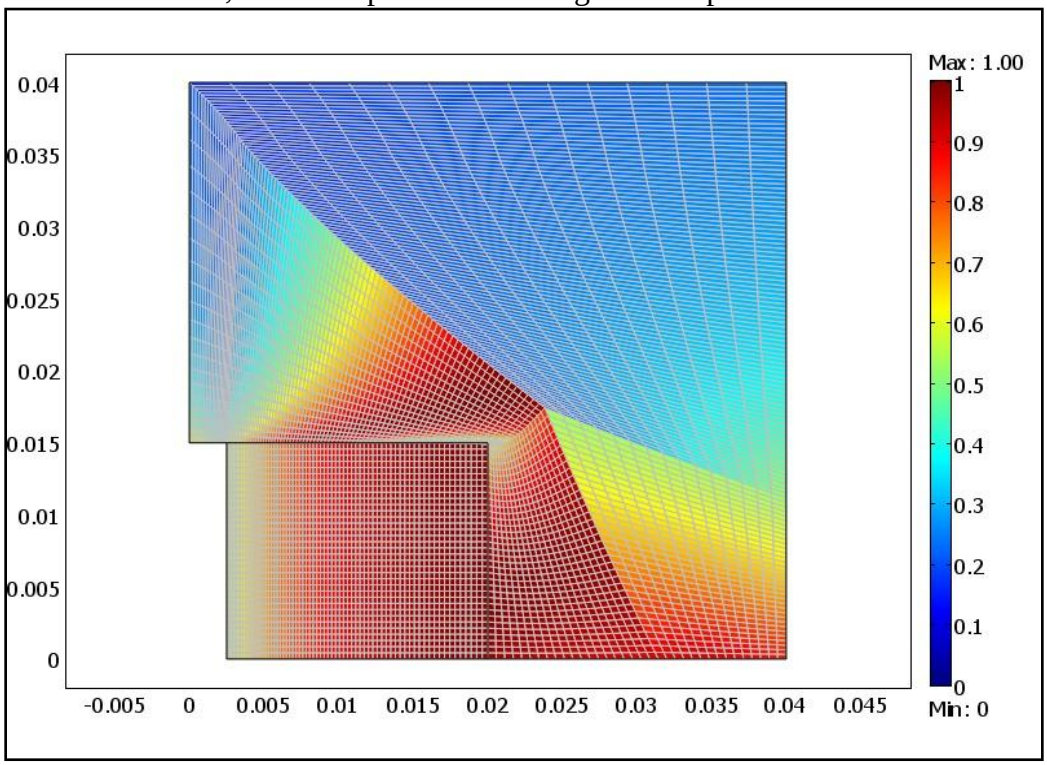

Figure 6.2.3. Mesh Quality: The element quality of each element in the final mesh. This plot shows that in the region of interest (the prostate) the quality is fairly high, but it is lower in the surrounding tissue.

6.3 Appendix C: Additional Visuals

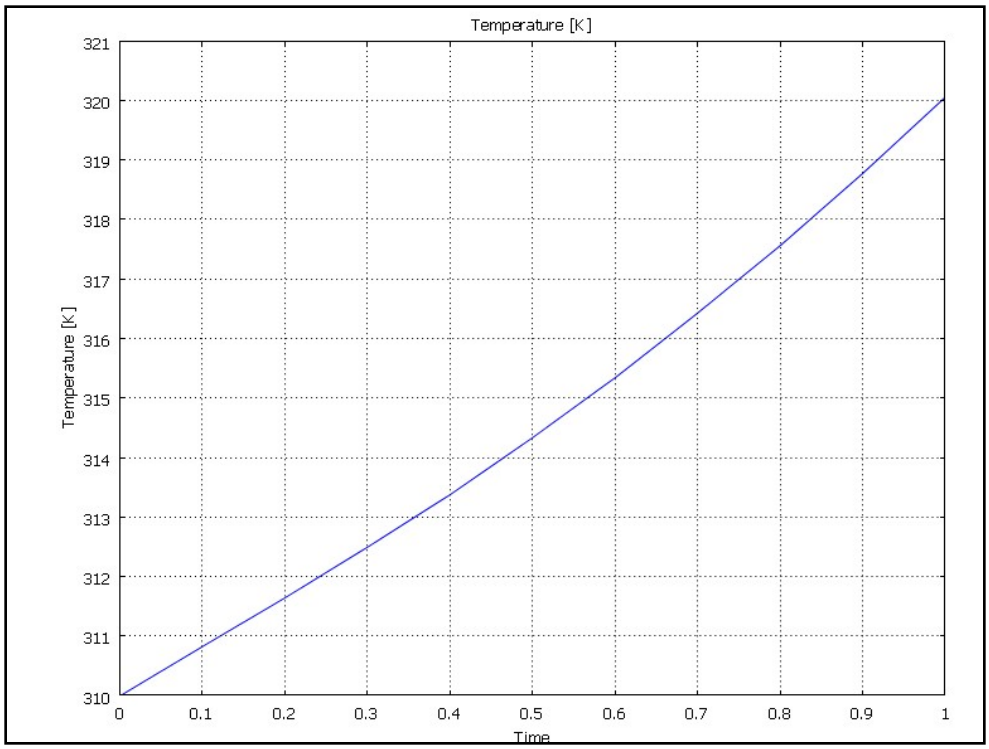

Figure 6.3.1. Temporal Temperature Change: Plot of temperature at point (.005, .005) for a time of 1 second.

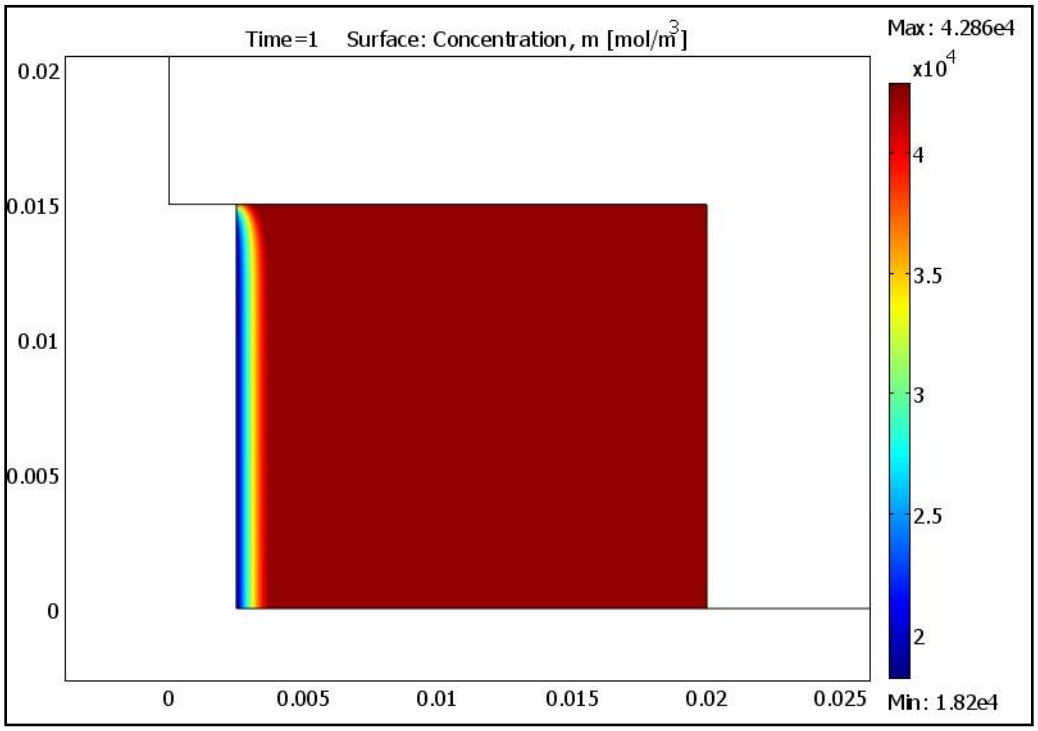

Figure 6.3.2. Water Concentration: Surface plot of the water concentration (mol/m^3) in the prostate after 1s of laser heating. Notice this high water concentration (shown in red) in most of the prostate. This is consistent with our temperature contour plot which indicates vaporization only in the first few millimeters of the prostate.

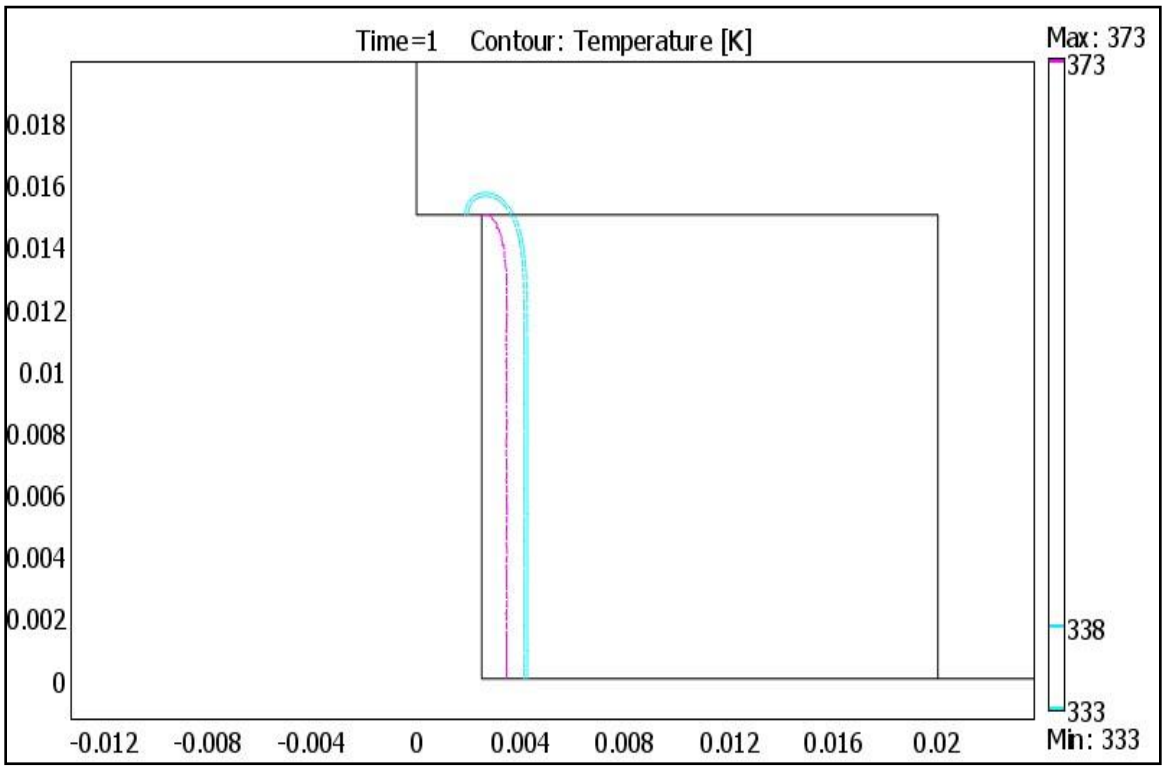

Figure 6.3.3. Contour Plot for 1 second at 60 W: Vaporization depth is 0.939 mm and the coagulation depth is 0.805 mm.

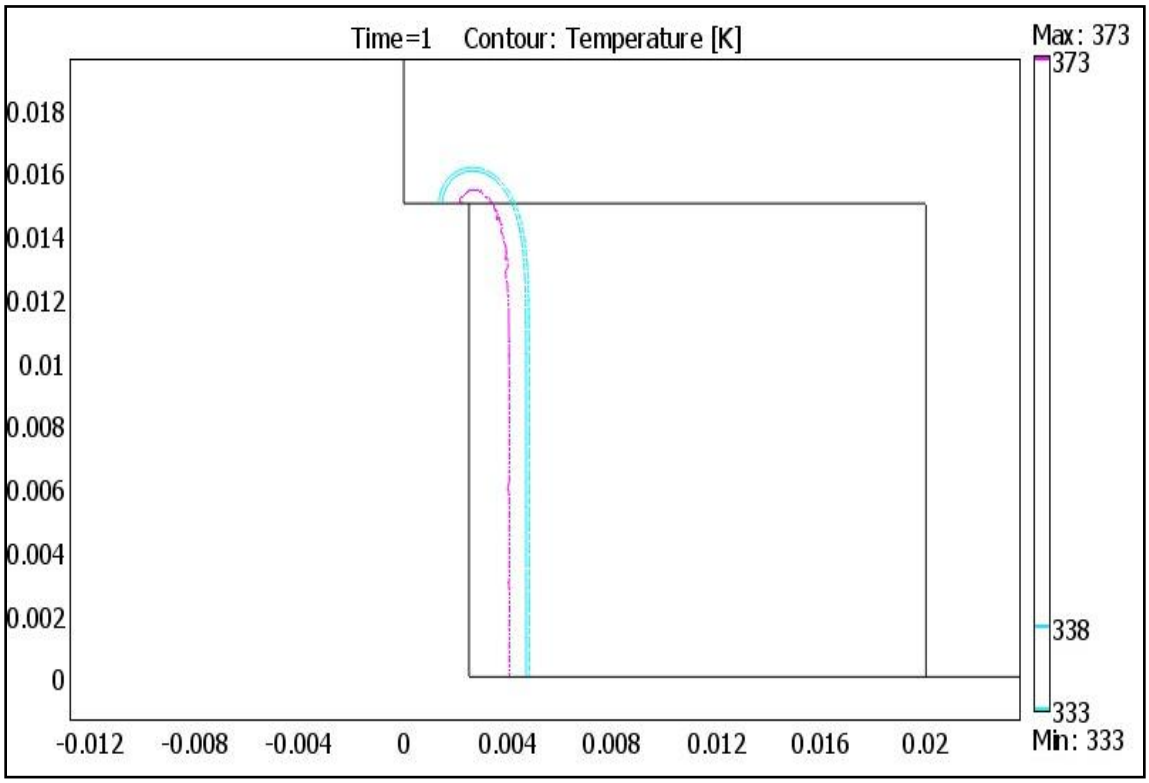

Figure 6.3.4. Contour Plot for 1 second at 120 W: Vaporization depth is 1.539mm and the coagulation depth is 0.761mm.

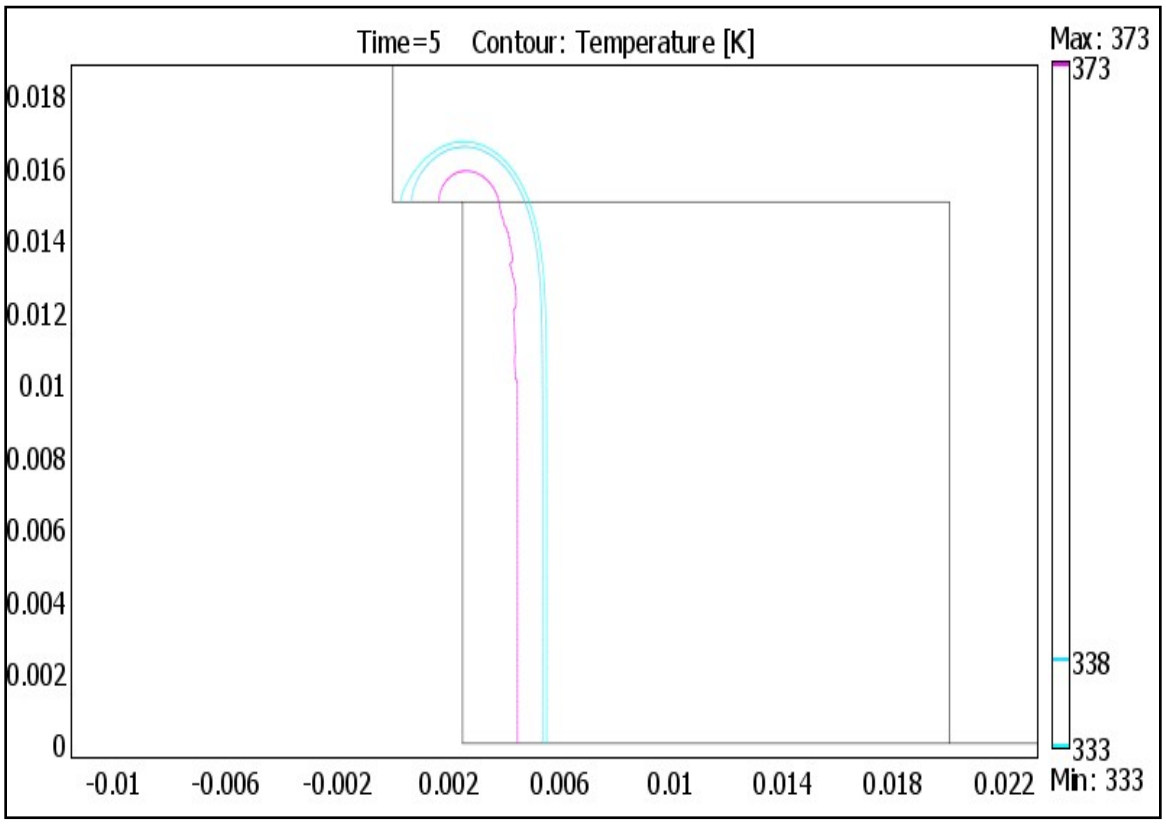

Figure 6.3.5. Contour plot for 5 seconds at 40W. Vaporization depth is 1.849mm and the coagulation depth is 1.171mm.

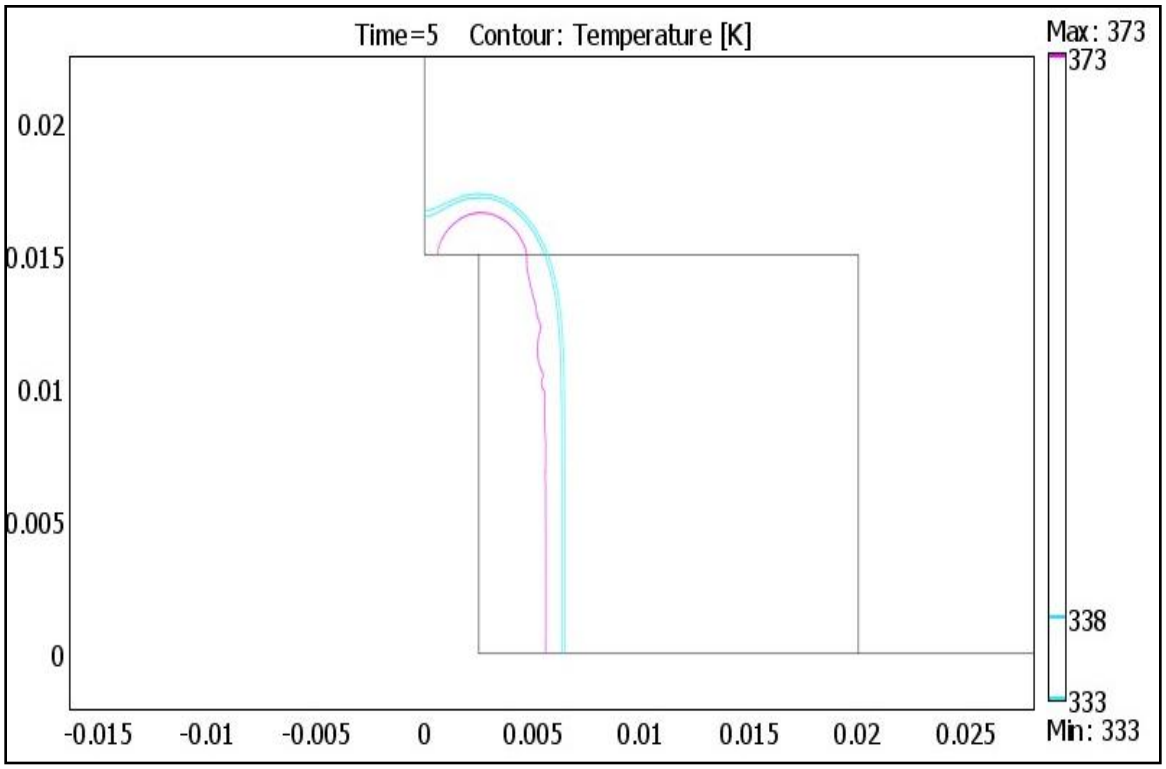

Figure 6.3.6. Contour plot for 5 seconds at 80W. Vaporization depth is measured to be 3.066 mm, and the coagulation depth is 0.892 mm.

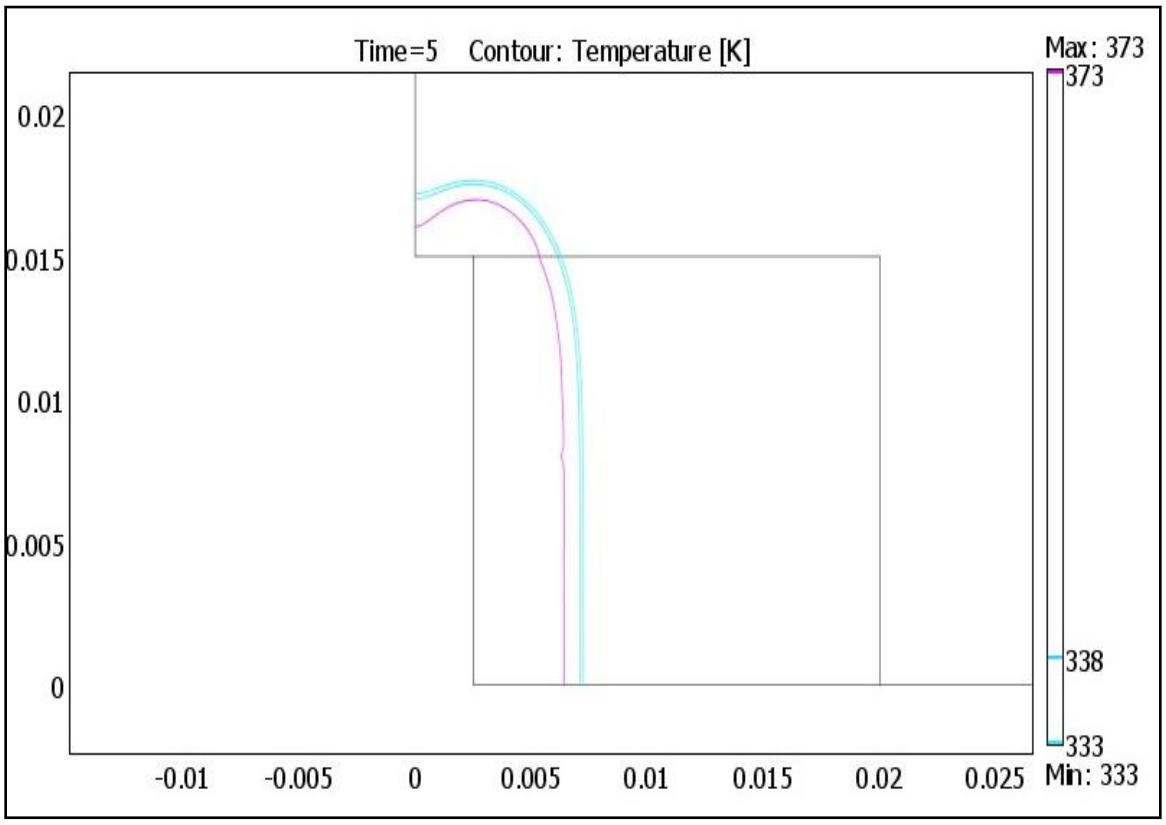

Figure 6.3.7. Contour plot for 5 seconds at 120W: Vaporization and coagulation depths are measured to be 3.893 mm and 0.797 mm, respectively.

6.4 Appendix D

References

1. Rubenstein, Jonathon, and McVary, Kevin T. 2008. Transurethral Microwave Thermotherapy of the Prostate (TUMP). Emedicine: Feb 6, 2008. http://emedicine.medscape.com/article/449623-overview
2. Berry, S.J., Coffey, D.S., Walsh, P.C., and Ewing, L.L. 1984. The development of human benign prostatic hyperplasia with age. *Journal of Urology* 132(3): 474-479.
3. Edwards J.L. 2008. Diagnosis and Management of Benign Prostatic Hyperplasia. *American Family Physician* 77(10): 1403.
4. Barry, M.J, Fowler, F.J., O'Leary, M.P., Bruskewitz, R.C., Mebust WK, Cockett AT. 1992. The American Urological Association symptom index for benign prostatic hyperplasia. The Measurement Committee of the American Urological Association. *Journal of Urology* 148(5):1549-57.
5. Malek, R., et. al. 2005. Photoselective Potassium-Titanyl-Phosphate Laser Vaporization of the Benign Obstructive Prostate: Observations on Long-Term Outcomes. *The Journal of Urology* 174:1344-1348.
6. Hai, Mahmood A. 2009. Photoselective Vaporization of Prostate: Five-year Outcomes of Entire Clinic Patient Population. *Urology* 73(4): 807-810.
7. Elzayat, E., et. al. 2007. Minimally Invasive Treatment of Benign Prostatic Hyperplasia: Laser. *American Urological Association Update Series* 26: 269-276.
8. Jacques, S. 1989. Time-Resolved Reflectance Spectroscopy in Turbid Tissues. *IEEE Transactions on Biomedical Engineering* 36:1155-1161.
9. Lee, R., et. al. 2006. The Evolution of Photoselective Vaporization Prostatectomy (PVP): Advancing the Surgical Treatment of Benign Prostatic Hyperplasia. *World Journal of Urology* 24:405-409.
10. Malek, R., et. al. 2005. Photoselective Potassium-Titanyl-Phosphate Laser Vaporization of the Benign Obstructive Prostate: Observations on Long-Term Outcomes. *The Journal of Urology* 174:1344-1348.
11. Seitz, M., et. al. 2009. High-power diode laser at 980nm for the treatment of benign prostatic hyperplasia: ex vivo investigations on porcine kidneys and human cadaver prostates. *Lasers Med Sci* 24:172-178.
12. Shafirstein, G., et. al. 2007. Modeling Photothermolysis for Optimizing Laser Treatments of Vascular Malformations. *Proceedings of the COMSOL Conference 2007*:1-7.
13. Sountoulides P, Tsakiris P. 2008. The Evolution of KTP Laser Vaporization of the Prostate. *Yonsei Medical Journal* 49(2):189-199.
14. Topaloglu, U., et.al. 2008. Virtual Thermal Ablation in the Head and Neck using Comsol MultiPhysics. *Proceedings of the COMSOL Conference 2008*;1-7.
15. Zhang, R., et. al. 2005. Comparison of Diffusion Approximation and Monte Carlo Based Finite Element Models for Simulating Thermal Responses to Laser Irradiation in Discrete Vessels. *Physics in Medicine and Biology* 50:4075-4086.
16. Alivizatos G, Skolarikos A. 2007. Photoselective Vaporization of the Prostate. Review of Cost Implementation to BPH Treatment. *Prostate Cancer and Prostatic Diseases Nature Publishing Group* 10:S15-S20.
17. Lee R, et al. 2008. Photoselective Vaporization of the Prostate Using a Laser High Performance System in the Canine Model. *The Journal of Urology* 180:1551-1553.